FERROELECTRICS
2019, VOL. 538, 135–144
https://doi.org/10.1080/00150193.2019.1569996

Taylor & Francis
Taylor & Francis Group

Structural, Electronic, and Mechanical Properties of $A_3Mn_2O_7$ (A = Sr, Ca): Ab Initio Calculation

Sevket Simsek[a], Husnu Koc[b], Amirullah M. Mamedov[c,d], and Ekmel Ozbay[c]

[a]Faculty of Engineering, Department of Material Science and Engineering, Hakkari University, Hakkari, Turkey; [b]Faculty of Sciences, Department of Physics, Siirt University, Siirt, Turkey; [c]Nanotechnology Research Center, Bilkent University, Ankara, Turkey; [d]International Scientific Center, Baku State University, Baku, Azerbaijan

ABSTRACT

In the present study, the structural, electronic, optical, and mechanical properties of the Ruddlesden-Popper type oxide compounds are investigated by means of density functional theory. In our calculation, spin polarized electron band structures and density of the state were identified by adding to the spin contribution of the Mn-atom. For $A_3Mn_2O_7$ compounds, the real and imaginary parts of the dielectric function and other optical properties, such as energy loss function, effective number of valence electrons, and effective optical dielectric constant, were calculated accordingly. In addition, the bulk modules, shear modules, Young's modulus and Poisson ratios, anisotropy factors, sound velocities, and Debye temperatures for these compounds were calculated too.

ARTICLE HISTORY
Received 14 May 2018
Accepted 13 October 2018

KEYWORDS
Ruddlesden-popper; electronic structure; elastic constants; first principles calculation

1. Introduction

Recently, there has been growing interest in the study of layered perovskites, which possess a wide variety of interesting properties, including superconductivity, colossal magnetoresistance (CMR) [1,2], ferroelectricity, and catalytic activity [3–12]. Layered perovskites are intergrowths of perovskite and other structures, and they consist of two dimensional (2D) perovskite slabs interleaved with cations or cationic structural units. Dion–Jacobson, Ruddlesden–Popper phases, and Aurivillius phases form the major families of the closely related layered perovskites. Among the manganese-based perovskite oxides, the layered Ruddlesden-Popper (R-P) manganite phase is of great interest for researchers. It was also reported that the some members of Ruddlesden-Popper (R-P) manganite phase have been hybrid improper ferroelectric (HIF) magnet properties [13–18]. R-P series are generally in $A_{n+1}B_nO_{3n+1}$ formula, where A site is occupied by an alkaline earth or rare earth metal ion such as Sr, Ca, Ba or La-Lu, B site is occupied by a transition metal ion like as Mn, Nb, Pb, Ti, Co and Ru, and n can take values from 1 to ∞. R-P phases can be also denoted by $(AO)(ABO_3)_n$ formula and their structure consist of n consecutive perovskite layers (ABO_3), alternating with

CONTACT Sevket Simsek ssimsek_001@hotmail.com
Color versions of one or more of the figures in the article can be found online at www.tandfonline.com/gfer.

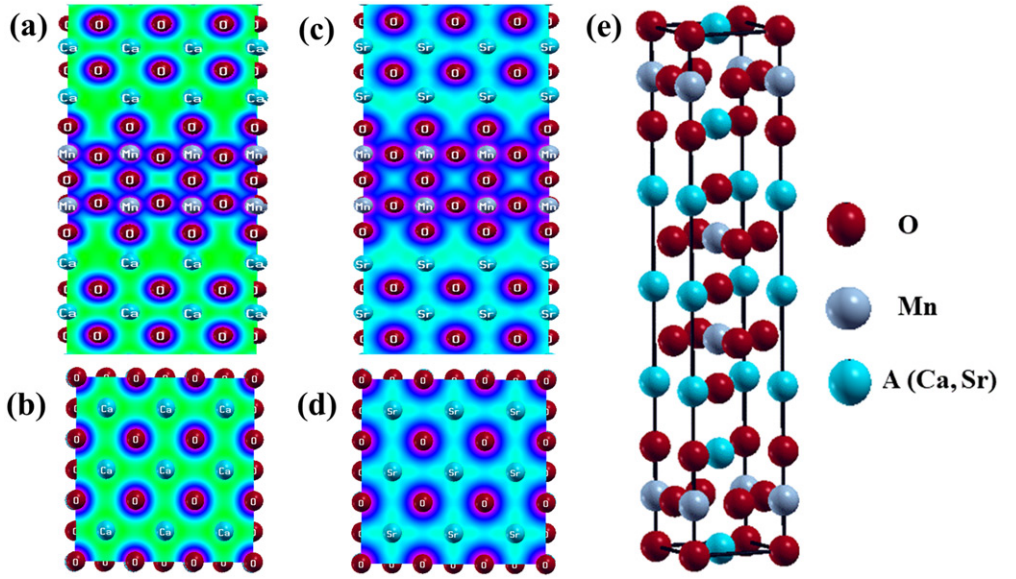

Figure 1. The calculated total charge density for (011) (a,c), (110) planes (b,d) and crystal structure (e) of $A_3Mn_2O_7$ compounds.

(AO) rock salt layers along the crystallographic c direction. While ABO_3 type perovskite structures correspond to n=∞, A_2BO_4 type structures such as K_2NiF_4, they are predicated by n = 1. $Sr_3Mn_2O_7$ and $Ca_3Mn_2O_7$ compounds are members of the R-P perovskite family corresponding to n = 2 [19–21].

$A_3Mn_2O_7$ (A:Sr, Ca) compounds have not been intensively studied apart from structural, electric, and magnetic measurement. As far as we know, an ab initio potential calculation has not been performed on the electronic, optical, and mechanical properties of $A_3Mn_2O_7$ compounds except a few articles [9, 22,23] in the literature. Therefore, the aim of our work is to present structural, electronic, optical, and mechanical properties of $A_3Mn_2O_7$ compounds by using density functional theory.

2. Method of Calculation

All calculations presented in this paper were carried out using the Vienna ab initio simulation package (VASP) code [24–27] by means of the density functional theory (DFT) [28]. The exchange-correlation energy function is treated within the spin polarized GGA (generalized gradient approximation) by the density functional of Perdew et al. [29]. To get good convergence, the kinetic energy cutoff for the total energy calculation is found to be 532 eV for $Ca_3Mn_2O_7$ and 554 eV for $Sr_3Mn_2O_7$. The $7 \times 7 \times 7$ for $Ca_3Mn_2O_7$ and $15 \times 15 \times 15$ for $Sr_3Mn_2O_7$ Monkhorst-Pack [30] mesh grids for electronic and structural calculations have been used for special **k** points in the Brillouin zone (BZ). The k-mesh grids are taken as $9 \times 9 \times 9$ for $Ca_3Mn_2O_7$ and $18 \times 18 \times 18$ for $Sr_3Mn_2O_7$ for the density of states (DOS) and optical spectra.

Table 1. The calculated and experimental lattice parameters for $Ca_3Mn_2O_7$ and $Sr_3Mn_2O_7$

Material	Reference	a (Å)	c (Å)
$Ca_3Mn_2O_7$	Present	3.7642	19.3187
	Cal. [23]	3.772	19.257
	Exp. [29]	3.6957	19.4873
	Exp. [45]	3.7072	19.4160
	Exp. [11]	3.6918	19.6254
	Exp. [21]	3.6834	19.5748
$Sr_3Mn_2O_7$	Present	3.8466	20.1900
	Exp. [3]	3.7894	20.0638

3. Results and Discussion

3.1. Structural Properties

The crystal structures of $Sr_3Mn_2O_7$ and $Ca_3Mn_2O_7$ are characterized with the tetragonal structure as seen in Fig. 1(e). These compounds have two molecules with 24 atoms in the unit cell. Firstly, we determined the structural parameters of $A_3Mn_2O_7$ compounds by relaxing the cell shape using experimental data [3, 31]. The obtained results are given in Table 1. We see that the results of our structural optimizations are in very close agreement with the experimental and previous calculated data.

3.2. Electronic Properties

The spin-polarized electronic band structures of the $A_3Mn_2O_7$ compounds were calculated using GGA along the high symmetry directions in the first Brillouin zone (BZ). The band structures and total density of states for majority spin (spin-up) and minority spin (spin-down) are shown in Fig. 2. As seen in Fig. 2(a, d), the Fermi level crosses the energy dispersion curves of majority spin states. Therefore, $A_3Mn_2O_7$ compounds show metallic properties for spin-up electrons. However, we can see in Fig. 2(b, e) that there is an indirect band gap of approx. 0.532 eV for $Ca_3Mn_2O_7$ and 0.663 eV for $Sr_3Mn_2O_7$ near the Fermi level for spin-down electrons and, therefore, the minority spin states of $A_3Mn_2O_7$ compounds have the semiconductor character. An indirect gap of $Sr_3Mn_2O_7$ in the antiferroelectric structure was reported as 0.45 eV in Ref [9]. This is smaller than our value. The partial and total DOS calculated for these compounds are illustrated in Fig. 2. For the $Sr_3Mn_2O_7$ compound, the lowest valance bands, valance bands between -50 eV and -30 eV as well as -20 eV and -10 eV, and upper most occupied valence bands are formed by Mn p and s states, the hybridization of Mn (p) and Sr (s)- states and hybridization of O (p)- Mn (d)-states. The situation occurring very close to it can be observed for the $Ca_3Mn_2O_7$ compound. The lowest unoccupied conduction band above the Fermi level for the both compounds are formed by the hybridization of the p and d states of Mn and Sr(Ca), but d states dominate.

In order to determine the bonding nature between atoms in $A_3Mn_2O_7$ compounds, we have calculated contour maps of the total electronic charge density for (011) and (110) planes as shown in Fig. 2(a–d). It is clear that there is strong covalent bonding between the Mn and O atoms. Whereas, Ca and Sr form an ionic bonding with O.

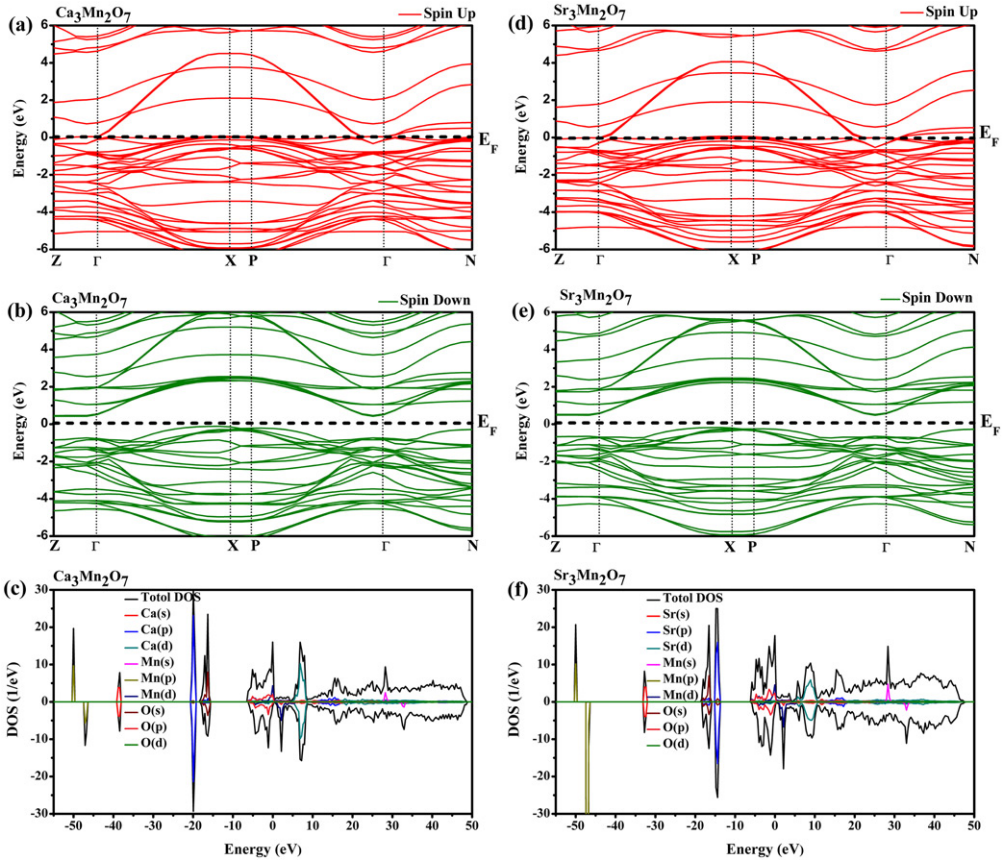

Figure 2. The calculated electronic band structures and total density of states for the majority spin (spin-up) and minority spin (spin-down) of $Ca_3Mn_2O_7$ (a,b and c) and $Sr_3Mn_2O_7$ (d, e and f) compounds.

3.3. Optical Properties

The calculated real ($\varepsilon_1(\omega)$) and imaginary ($\varepsilon_2(\omega)$) parts of dielectric functions and electron energy-loss spectrum for the $A_3Mn_2O_7$ compounds by using Kramers-Kroning relations [32–35] are shown in Fig. 3. As seen from Fig. 3, the energy values of $\varepsilon_1(\omega)$ that decreasing and increasing are zero 0.23 (0.23) eV and 7.80 (5.41) eV for x-direction and 4.50 (4.2) eV, and 1.78(1.88) eV for $Ca_3Mn_2O_7$ ($Sr3Mn_2O_7$) compounds. These values that $\varepsilon_1(\omega)$ are zero points reduced of the reflections, and show that the polarization disappears. The maximum peak values of $\varepsilon_2(\omega)$ are 0.12 eV, 2.37 eV and 4.50 eV for $Ca_3Mn_2O_7$, and 0.12 eV and 4.24 eV for $Sr_3Mn_2O_7$. These values show how much the electromagnetic wave polarizes the system, and corresponds to the electronic transitions from the valence band to the conduction band. Furthermore, as can be seen in Fig. 3, the approximately 0.1-7.0 eV energy region for both compounds, respectively, is the region where dispersion is low and also where we observe the intensive interband transition. The energy region above 10 eV corresponds to the collective vibration of valance electrons. This energy region defined as plasma oscillations is described by the energy loss function.

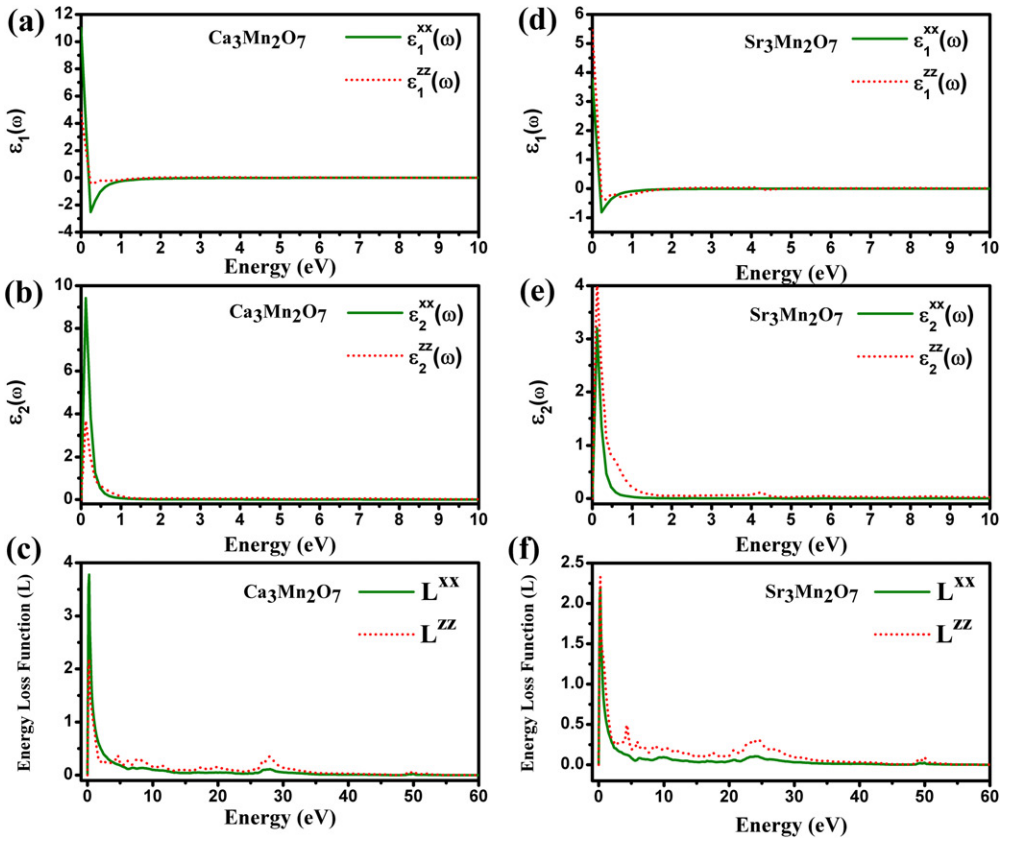

Figure 3. The calculated reel and imaginary parts of dielectric functions and electron energy-loss spectrum for the $A_3Mn_2O_7$ compounds.

The calculated effective number (N_{eff}) of electrons participating in the interband transitions and effective optical dielectric constant (ε_{eff}) for the $A_3Mn_2O_7$ compounds are given in Fig. 4. The ε_{eff} reaches a saturation value at approximately 1.0 eV for both compounds, this means that the greatest contribution to ε_{eff} from the interband transitions between 0.1 eV and 1.5 eV. The N_{eff} reaches the saturation value at energy above 30 eV. This means that deep-lying valence orbitals participate in interband transitions as well.

3.4. Elastic Properties

Elastic constants contain information about many important properties of solids, such as the brittle and ductile, mechanical stability, specific heat, Debye temperature, thermal expansion coefficient, and bonding nature between atoms [36,37]. The elastic constants of $Ca_3Mn_2O_7$ and $Sr_3Mn_2O_7$ compounds were calculated using the strain–stress method [38] as implemented in the VASP [24, 27]. For tetragonal crystals, there are six independent elastic constants namely, C_{11}, C_{12}, C_{13} C_{33}, C_{44} and C_{66}. The bulk modules, shear modules, Young's modulus and Poisson ratios, anisotropy factors, sound velocities, and Debye temperatures of $A_3Mn_2O_7$ compounds have been calculated using the common relations given in Ref. [39–42]. The results are listed in Tables 2, 3, and 4.

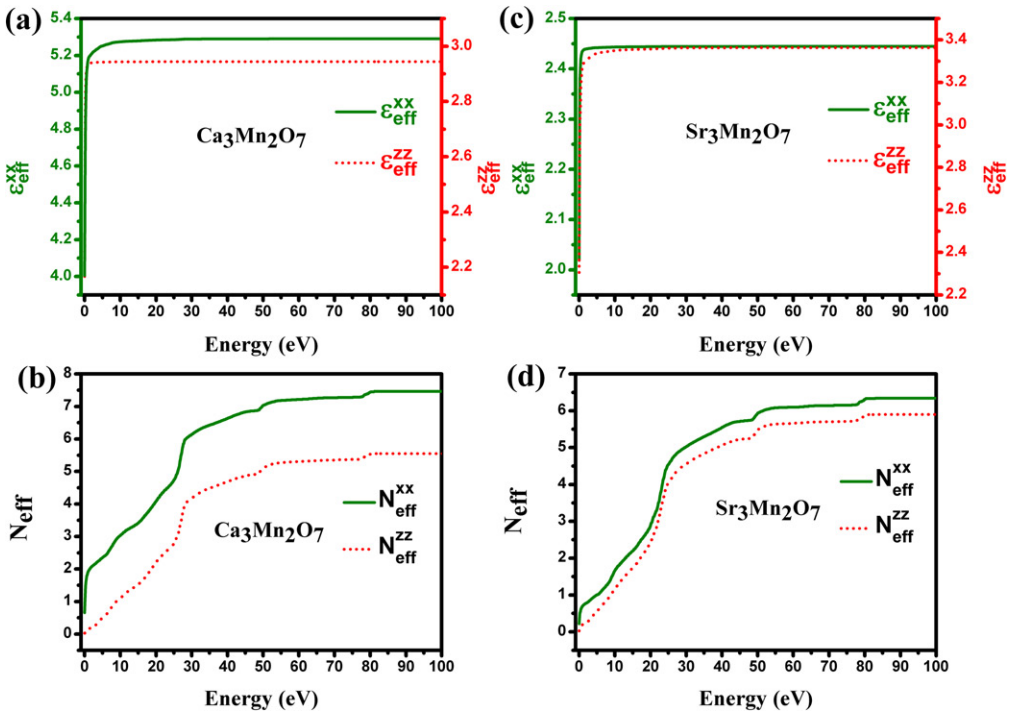

Figure 4. The calculated effective number (N_{eff}) of electrons participating in the interband transitions and effective optical dielectric constant (ε_{eff}) for the $A_3Mn_2O_7$ compounds.

The calculated elastic constants in Table 2 satisfy the mechanical stability conditions given in Ref [39] for tetragonal crystals. It indicates that both compounds are mechanically stable. It is well known that the elastic constants C_{11}, C_{22}, and C_{33} measure the a-, b-, and c direction resistance to linear compression, respectively [42]. We can see from Table 2 that the values of C_{11} are smaller than C_{33} for both materials. For this reason, $A_3Mn_2O_7$ compounds are more compressible along the a-axis.

Besides, our calculated C_{11}, C_{13}, and C_{44} values are in good agreement with the calculated values using the GGA approaches in Ref. [23]. However, C_{12}, C_{33}, and C_{66} values are bigger than the obtained values in Ref. [23].

While the bulk modulus (B) is a measure of the resistance of the material to volume change under an applied pressure, the isotropic shear modulus (G) is a measure of the resistance to reversible deformations caused by shear strain. The calculated bulk modulus values are 158.26 GPa and 142.86 GPa for $Ca_3Mn_2O_7$ and $Sr_3Mn_2O_7$, respectively. Thus, these materials can be expressed as a medium hardness material. Because the bulk and shear modulus of $Ca_3Mn_2O_7$ are smaller than that of $Sr_3Mn_2O_7$, one can say that $Ca_3Mn_2O_7$ is a less compressible compound than $Sr_3Mn_2O_7$. In addition, The Young's modulus indicates the hardness of the materials. The Young's modulus of $A_3Mn_2O_7$ compounds was calculated to be as 242.18 GPa ($Sr_3Mn_2O_7$) and 227.58 GPa ($Sr_3Mn_2O_7$). Thus, these materials exhibit a low stiffness.

Poisson's ratio can take different values depending on the nature of bonding in materials. It reflects the degree of directionality of the covalent bonds. While values of Poisson's ratio (υ) is 0.1 for the covalent material, for ionic material it is 0.25, and for

Table 2. The calculated elastic constants (in GPa) for $A_3Mn_2O_7$ compounds

	$Ca_3Mn_2O_7$				$Sr_3Mn_2O_7$
	GGA	GGA and GGA + U from Ref [23]			GGA
	This work	U = 0 eV	U = 3.5 eV	U = 5 eV	This work
C_{11}	304.58	305.649	267.496	265.031	252.92
C_{12}	73.89	67.568	56.549	45.967	82.09
C_{13}	87.47	88.550	81.191	75.574	86.41
C_{33}	318.62	285.819	281.988	278.956	272.17
C_{44}	83.07	81.683	81.556	78.477	93.44
C_{66}	98.60	81.814	78.767	78.095	100.30

Table 3. The calculated isotropic bulk modulus (B, in GPa), shear modulus (G, in GPa), Young's modulus (E, in GPa), and Poisson's ratio for $A_3Mn_2O_7$compounds

	$Ca_3Mn_2O_7$				$Sr_3Mn_2O_7$
	GGA	GGA and GGA + U from Ref [23]			GGA
	This work	U = 0 eV	U = 3.5 eV	U = 5 eV	This work
B_V	158.38	154.050	139.427	133.694	143.09
B_R	158.13	154.050	138.823	132.951	142.86
B	158.26	154.050	139.125	133.323	142.98
G_V	98.21	92.533	88.245	87.803	92.31
G_R	96.31	90.471	87.110	86.106	92.01
G	97.26	91.502	87.678	86.954	92.16
E	242.18	229.138	217.370	214.278	227.58
N	0.24	0.252	0.240	0.232	0.23
B/G	1.62	1.684	1.587	1.533	1.55

Table 4. The transverse, longitudinal, average elastic wave velocities (v_t, v_l and v_m, in m/s), density (ρ in g/cm^3), Debye temperature (Θ_D in K), shear anisotropic factors A_1, A_2, A_3, and $A_{comp(\%)}$, $A_{shear(\%)}$ for $A_3Mn_2O_7$compounds

Compound	v_t	v_l	v_m	ρ	Θ_D(K)	A_1	A_2	A_3	Acomp(%)	Ashear(%)
$Ca_3Mn_2O_7$	4841.2	8329.8	5371.5	4.15	710.5	0.74	0.77	0.85	0.08	0.97
$Sr_3Mn_2O_7$	4135.0	7023.1	4582.5	5.39	588.7	1.06	1.01	1.17	0.08	0.16

the metallic material it is 0.33 [43]. The calculated Poisson's ratio values for $Ca_3Mn_2O_7$ and $Sr_3Mn_2O_7$ are approx. 0.24 and 0.23, respectively. Therefore, the ionic contribution to inter atomic bonding for both materials is more dominant. On the other hand, as we can see from the Table 3, our results are very close to the calculated values in Ref. [23]. But, the calculated values using the GGA + U approaches in Ref. [23] are smaller than our obtained values.

As stated in Pugh's criterion [44], B/G ratio can be used to determine the ductile ($B/G > 1.75$) or brittle behavior ($B/G < 1.75$) of the materials. Because the calculated values of the B/G for $A_3Mn_2O_7$ compounds are smaller than 1.75, these compounds behave as brittle manner.

On the other hand, the elastic anisotropy is an important parameter that is related to the elastic properties of solids. The bonding natures in different crystallographic directions and microcrack formation in materials can be determined via elastic anisotropy [32]. The calculated anisotropic factors are given in Table 4. The values of the anisotropic factors (A_1, A_2 and A_3) are equal to 1 for an isotropic crystal. If their values are smaller or greater than 1, the crystal exhibits an anisotropic character. It is clear in

Table 4 that, while the $Sr_3Mn_2O_7$ compound shows a weak anisotropy, the $Ca_3Mn_2O_7$ compound indicates a strong anisotropy.

Another way of describing the elastic anisotropy is to calculate the percentage of anisotropy in the compression and shear. For crystals, these values can vary from zero (isotropic) and 100% representing the maximum anisotropy [42]. As seen in Table 4, the anisotropy in compression for both compounds is small. However, while the anisotropy in shear for $Ca_3Mn_2O_7$ is high, it is small for $Sr_3Mn_2O_7$.

The Debye temperature (Θ_D) is related to many fundamental physical properties of solids such as the specific heat, melting temperature, phonos, elastic constants, and vibrational entropy. At low temperatures, the Debye temperature can be calculated from the elastic constants [32]. The calculated Debye temperature for both compounds is listed in Table 4. It is clear that the calculated Debye temperature of $Ca_3Mn_2O_7$ is higher than $Sr_3Mn_2O_7$.

4. Conclusion

In this work, we have investigated the structural, electronic, optic, and mechanical properties of the $Ca_3Mn_2O_7$ and $Sr_3Mn_2O_7$ crystals by means of the density functional theory. The electronic band calculation results show that majority spin states for both compounds exhibit metallic properties for spin-up electrons. However, minority spin states for both compounds show semiconductor properties. We have also calculated the mechanical properties such as bulk modulus, shear modulus, Young's modulus, Poisson's ratio, Debye temperature, and shear anisotropic factors. According to the obtained results, both materials are mechanically stable, and can be expressed as a medium hardness material. Moreover, the ionic contribution to inter atomic bonding for these compounds is dominant. We have also made some comparisons with related experimental and theoretical data that were available.

Acknowledgements

This work is supported by the projects DPT-HAMIT and NATO-SET-193 as well as by the Hakkari University Scientific Research Projects Coordination Unit (Project Number: MF18BAP7). One of the authors (Ekmel Ozbay) acknowledges partial support from the Turkish Academy of Sciences.

References

1. N. Mahamdioua *et al.*, Magneto-conductive mechanisms in the La-site doped double-layered $La_{1.4}Ca_{1.6}Mn_2O_7$ manganites. *Physica B.* **500**, 77 (2016). DOI: 10.1016/j.physb.2016.07.011.
2. H. Tanaka, and T. Kawai, Artificial construction of layered perovskite superlattice by laser molecular-beam epitaxy. *Appl. Phys. Lett.* **76**(24), 3618 (2000). DOI: 10.1063/1.126725.
3. J. F. Mitchell *et al.*, $Sr_3Mn_2O_7$: Mn^{4+} Parent Compound of the n = 2 Layered CMR Manganites. *J. Solid State Chem.* **141**(2), 599 (1998). : DOI: 10.1006/jssc.1998.8026.
4. Y. Konishi *et al.*, Fabrication and physical properties of c-axis oriented thin films of layered perovskite $La_{2-2x}Sr_{1+2x}Mn_2O_7$. *Appl. Phys. Lett.* **73**(20), 3004 (1998). DOI: 10.1063/1.122658.

5. P. Fris *et al.*, Direct observation of double exchange in ferromagnetic $La_{0.7}Sr_{0.3}CoO_3$ by broadband ellipsometry. *Phys. Rev. B.* **97**, 045137 (2018).
6. R. Chihoub *et al.*,Magneto resistive properties of cerium doped $La_{0.7}Ca_{0.3}MnO_3$ manganites. *Physica B.* **492**, 11 (2016). DOI: 10.1016/j.physb.2016.03.031.
7. S. P. Altintas *et al.*, Effect of anionic substitution on the structural and magneto-electrical properties of La–Ca–Mn–O perovskite manganites. *J. Magn. Magn. Mater.* . **368**, 111 (2014). DOI: 10.1016/j.jmmm.2014.05.010.
8. N. Mahamdioua *et al.*, Structural and magnetotransport properties of the Y doped A-site deficient double layered manganites $La_{1.2\_x}\square_{0.2}Y_xCa_{1.6}Mn_2O_7$. *J. Solid State Chem.* **240**, 1 (2016). DOI: 10.1016/j.jssc.2016.05.011.
9. H. Meskine, Z. S. Popovic, and S. Satpathy, Electronic structure and exchange interaction in the layered perovskite $Sr_3Mn_2O_7$. *Phys. Rev. B.* **65**, 094402 (2002).
10. K. Raju, M. S. Song, and J. Y. Lee, Crystal structure and magnetic properties of $La_{2\_x}(Sr_{0.5}Ca_{0.5})_{1+x}Mn_2O_7$ (x = 0.6, 0.8 and 1.0) Ruddlesden–Popper manganites. *J. Magn. Magn. Mater.* **358**, 119 (2014). DOI: 10.1016/j.jmmm.2014.01.040.
11. M. V. Lobanov *et al.*, Crystal and magnetic structure of the $Ca_3Mn_2O_7$ Ruddlesden–Popper phase: neutron and synchrotron x-ray diffraction study. *J. Phys: Condens. Matter* . **16**, 5339 (2004). DOI: 10.1088/0953-8984/16/29/023.
12. X. Zhang *et al.*, Novel optical and magnetic properties of Li-doped quasi-2D manganate $Ca_3Mn_2O_7$ particles. *J. Mater. Chem. C.* **5**(28), 7011 (2017). DOI: 10.1039/C7TC01667K.
13. W. Zhu *et al.*, Electrically induced decrease of magnetization in $Ca_3Mn_2O_7$. *Appl. Phys. Lett.* **101**(19), 192407 (2012). DOI: 10.1063/1.4767139.
14. N. A. Benedek, and C. J. Fennie, Hybrid improper ferroelectricity: a mechanism for controllable polarization-magnetization coupling. *Phys. Rev. Lett.* **106**, 107204 (2011).
15. T. Mulder *et al.*, Turning ABO_3 Antiferroelectrics into Ferroelectrics: Design Rules for Practical Rotation-Driven Ferroelectricity in Double Perovskites and $A_3B_2O_7$ Ruddlesden-Popper Compounds. *Adv. Funct. Mater.* **23**, 4810 (2013).
16. B. Gao *et al.*, Interrelation between domain structures and polarization switching in hybrid improper ferroelectric $Ca_3(Mn,Ti)_2O_7$. *Appl. Phys. Lett.* **110**(22), 222906 (2017). : DOI: 10.1063/1.4984841.
17. X. Q. Liu *et al.*, Hybrid improper ferroelectricity in Ruddlesden-Popper $Ca_3(Ti,Mn)_2O_7$ ceramics. *Appl. Phys. Lett.* **106**(20), 202903 (2015). : DOI: 10.1063/1.4921624.
18. J. G. Cherian *et al.*, Optical spectroscopy and band gap analysis of hybrid improper ferroelectric $Ca_3Ti_2O_7$. *Appl. Phys. Lett.* **108**(26), 262901 (2016).
19. X. Li *et al.*, Ultra-low coercive field of improper ferroelectric $Ca_3Ti_2O_7$ epitaxial thin films. *Appl. Phys. Lett.* **110**(4), 042901 (2017). DOI: 10.1063/1.4974217.
20. M. Greenblatt, Ruddlesden-Popper $Ln_{n+1}Ni_nO_{3n+1}$ nickelates: structure and properties. *Curr. Opin. Solid State Mater. Sci.* **2**, 174 (1997). DOI: 10.1016/S1359-0286(97)80062-9.
21. I. D. Fawcett *et al.*, Structure, magnetism, and properties of Ruddlesden-popper calcium manganates prepared from citrate gels. *Chem. Mater.* **10**, 3643 (1998).
22. S. F. Matar *et al.*, First-principles study of the electronic and magnetic structures of the tetragonal and orthorhombic phases of $Ca_3Mn_2O_7$. *Phys. Rev. B.* **76**, 054403 (2007).
23. Z. Wei, and T. Pei-Qing, A first-principles study of the structural and elastic properties of orthorhombic and tetragonal $Ca_3Mn_2O_7$. *Chin. Phys. B.* **22**, 066201 (2013).
24. G. Kresse, and J. Hafner, Ab initio molecular dynamics for liquid metals. *Phys. Rev. B.* **47**(1), 558 (1993). DOI: 10.1103/PhysRevB.47.558.
25. G. Kresse, and J. Furthmuller, Ab-initio total energy calculations for metals and semiconductors using a plane-wave basis set. *Comput. Mater. Sci.* **6**(1), 15 (1996). DOI: 10.1016/0927-0256(96)00008-0.
26. G. Kresse, and D. Joubert, From ultrasoft pseudopotentials to the projector augmented-wave method. *Phys. Rev. B.* **59**(3), 1758 (1999). DOI: 10.1103/PhysRevB.59.1758.

27. G. Kresse, and J. Furthmuller, Efficient iterative schemes for ab initio total-energy calculations using a plane-wave basis set. *Phys. Rev. B*. **54**(16), 11169 (1996). DOI: 10.1103/PhysRevB.54.11169.
28. P. Hohenberg, and W. Kohn, Inhomogeneous electron gas. *Phys. Rev*. **136**, A1133 (1964).
29. J. P. Perdew, S. Burke, and M. Ernzerhof, Generalized gradient approximation made simple. *Phys. Rev. Lett*. **77**(18), 3865 (1996). DOI: 10.1103/PhysRevLett.77.3865.
30. H. J. Monkhorst, and J. D. Pack, Special points for Brillouin-zone integrations. *Phys. Rev. B*. **13**(12), 5188 (1976). DOI: 10.1103/PhysRevB.13.5188.
31. J. L. Zhu *et al.*, La-doping and external pressure effects on the crystal structure of layered perovskite-like manganate $Ca_3Mn_2O_7$. *Phys. Stat. Sol. (a)*. **194**(1), 159 (2002). DOI: 10.1002/1521-396X(200211)194:1<159::AID-PSSA159>3.0.CO;2-9.
32. N. Guechi *et al.*, Structural, elastic, electronic and optical properties of the newly synthesized monoclinic Zintl phase $BaIn_2P_2$. *Solid State Sci*. **29**, 12 (2014). DOI: 10.1016/j.solidstatesciences.2014.01.001.
33. M. Xu *et al.*, Optical properties of cubic Ti_3N_4, Zr_3N_4 and Hf_3N_4. *Appl. Phys. Lett*. **89**(15), 151908 (2006). DOI: 10.1063/1.2360937.
34. Y. Shen, and Z. Zhou, Structural, electronic, and optical properties of ferroelectric $KTa_{1/2}Nb_{1/2}O_3$ solid solutions. *J. Appl. Phys*. **103**(7), 074113 (2008). DOI: 10.1063/1.2902433.
35. M. Dadsetani, and A. Pourghazi, Optical properties of strontium monochalcogenides from first principles. *Phys. Rev. B*. **73**, 195102 (2006).
36. E. Deligoz, and H. Ozisik, Mechanical and dynamical stability of TiAsTe compound from ab initio calculations. *Philos. Mag*. **95**(21), 2294 (2015). DOI: 10.1080/14786435.2015.1056854.
37. P. Bhardwaj, and S. Singh, First principle calculation of structural, electronic and elastic properties of rare earth nitride. *Mater. Sci.-Poland*. **34**(4), 715 (2016). DOI: 10.1515/msp-2016-0123.
38. Y. Le Page, and P. Saxe, Symmetry-general least-squares extraction of elastic coefficients from ab initio total energy calculations. *Phys. Rev. B*. **63**, 174103 (2001).
39. Z. J. Wu *et al.*, Crystal structures and elastic properties of superhard IrN_2 and IrN_3 from first principles. *Phys. Rev. B*. **76**, 054115 (2007).
40. H. Koc *et al.*, First principles prediction of the elastic, electronic, and optical properties of Sb_2S_3 and Sb_2Se_3 compounds. *Solid State Sci*. **14**(8), 1211 (2012). DOI: 10.1016/j.solidstatesciences.2012.06.003.
41. M. X. Zeng *et al.*, Elastic and electronic properties of tI26-type Mg12RE (RE = Ce, Pr and Nd) phases. *Model. Simul. Mater. Sci. Eng*. **20**(3), 035018 (2012). DOI: 10.1088/0965-0393/20/3/035018.
42. U. F. Ozyar, E. Deligoz, and K. Colakoglu, Systematic study on the anisotropic elastic properties of tetragonal XYSb (X = Ti, Zr, Hf; Y = Si, Ge) compounds. *Solid State Sci*. **40**, 92 (2015). DOI: 10.1016/j.solidstatesciences.2015.01.001.
43. J. Haines, J. M. Leger, and G. Bocquillon, Synthesis and design of superhard materials. *Annu. Rev. Mater. Res*. **31**(1), 1 (2001). DOI: 10.1146/annurev.matsci.31.1.1.
44. S. F. Pugh, Relations between the elastic moduli and the plastic properties of polycrystalline Pure Metals. *Lond. Edinb. Dublin Philos. Mag. J. Sci*. **45**(367), 823 (1954). DOI: 10.1080/14786440808520496.
45. T. Toyota *et al.*, High-temperature thermoelectric property of layered $La_{2-2x}Ca_{1+2x}Mn_2O_7$ manganites ($0.75 \leq x \leq 1.0$). *Jpn. J. Appl. Phys*. **50**, 041101 (2011). DOI: 10.7567/JJAP.50.041101.